Denoising Refinement Diffusion Models for Simultaneous Generation of Multi-scale Mobile Network Traffic

Xiaoqian Qi*, Haoye Chai^{†§}, Sichang Liu*, Lei Yue[‡], Raoyuan Pan[‡], Yue Wang*, Yong Li*

[†]Beijing University of Posts and Telecommunications, Beijing, China

*Department of Electronic Engineering, BNRist, Tsinghua University, Beijing, China

[‡]China Mobile Communications Group Guangxi Co., Ltd., Nanning, China

[†]{haoyechai}@bupt.edu.cn

*{qixiaoqian24, liusc22}@mails.tsinghua.edu.cn, {wangyue, liyong07}@tsinghua.edu.cn

[‡]{yuelei, panraoyuan}@gx.chinamobile.com

Abstract-Multi-layer mobile network traffic generation is a key approach to capturing multi-scale network dynamics, supporting network planning, and promoting generative management of mobile data. Existing methods focus on generating network traffic with a single spatiotemporal resolution, making it difficult to achieve joint generation of multi-scale traffic. In this paper, we propose ZoomDiff, a diffusion-based multiscale mobile traffic generation model. ZoomDiff maps the urban environmental context into network traffic with multiple spatiotemporal resolutions through custom-designed Denoising Refinement Diffusion Models (DRDM). DRDM employs a multistage noise-adding and denoising process, enabling different stages to generate traffic with distinct spatial and temporal resolutions. It aligns the progressive denoising process of diffusion models with hierarchical network layers, including BSs, cells, and grids with different granularities. Evaluations on real-world mobile traffic datasets demonstrate that ZoomDiff achieves a performance improvement of at least 18.4% over state-of-theart baselines on generation tasks at multi-scale traffic. The efficiency and generalization ability are also demonstrated, which indicates that ZoomDiff holds strong potential for generative mobile data management. The code of ZoomDiff is available at https://anonymous.4open.science/r/ZoomDiff-105E/.

Index Terms—Multi-scale mobile traffic, diffusion models, noise prior guidance

I. INTRODUCTION

Mobile network traffic serves as a vital indicator of both user behavior and network performance [1]. Accurate modeling and understanding of traffic dynamics not only reflect underlying communication activities but also inform essential decisions in network planning and optimization. However, the privacy of communication data and the imperfection of mobile traffic data management makes it difficult to obtain accurate and large-scale traffic datasets. Generative approaches can supplement scarce real-world measurements, enhance simulation fidelity, and accelerate the design and testing of network control strategies in a cost-effective and privacy-preserving manner [2]. This supports a variety of downstream optimization tasks such

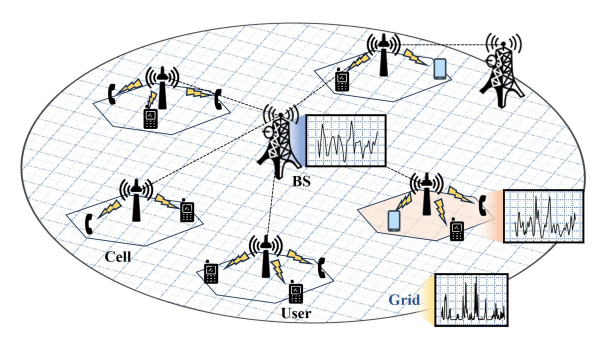


Fig. 1: Typical cellular mobile network, with multi-layer network nodes including BSs, cells, and users. Grids are aggregations of users within regularly defined geographical areas. The curves in the figure illustrate BS, cell, and grid traffic patterns with different temporal and spatial resolutions.

as Base Station (BS) deployment [3]–[6], resource management [7], [8], traffic load balancing [9], [10], and energy-efficient scheduling [11].

Over the past decade, extensive efforts have been devoted to generating mobile traffic data across various spatial scales, ranging from city-wide aggregation to regional and BS level granularity [12]–[15]. Such work typically leverages historical traffic patterns and statistical modeling approaches to simulate spatiotemporal traffic characteristics at diverse granularities. These studies lay foundational groundwork by adequately addressing macroscopic traffic generation demands and demonstrating their value in multiple practical network scenarios [16]–[18].

However, with the escalating complexity of networks and the emergence of novel mobile services such as immersive XR, autonomous driving, and tactile Internet [19]–[21], the demand for mobile traffic data generation exhibits two major trends. *First, multi-scale traffic generation*. The typical structure of a cellular mobile network, as shown in Fig. 1, consists of multiple layers of network nodes, including BSs, cells, grids, and users. As network structures become more

[§]Corresponding author.

complex, joint optimization across multiple network layers can yield greater performance gains compared with traditional single-layer strategies. This trend requires the support of synthetic traffic across multiple network layers with different spatiotemporal resolutions, while the intrinsic spatiotemporal correlations among these layers impose stringent requirements on the cross-layer organization and management of such data. **Second, high-resolution traffic generation.** High-resolution traffic patterns at fine spatial granularities, such as grid-level data, are increasingly critical for precision-based network optimization, including micro-level capacity planning, finegrained coverage optimization, and user-centric network configuration [22], [23]. Yet traffic at refined scales often exhibits intricate spatiotemporal dependencies and distributional complexities, which require generation-based data management systems to effectively capture and model fine-grained spatial correlations and rapid temporal variations in network dynamics.

Unfortunately, the aforementioned research can only generate coarse-grained network traffic with the same single spatiotemporal resolution as the training set. When generating and updating multi-scale traffic data, different models must be used to simulate different network layers, which greatly increases computational overhead. Moreover, generating the complex spatiotemporal distribution of fine-grained traffic exceeds the capabilities of existing methods. It requires advanced user localization techniques [24] or specialized network probes [25], incurring substantial communication overhead and computational costs [26], [27], making it infeasible for continuous collection in large-scale live networks. A promising yet largely unexplored alternative is to design a unified model capable of jointly generating multi-scale mobile traffic, allowing the easily estimated coarse spatiotemporal granularity traffic to progressively guide the generation of finer-grained traffic, thereby achieving multi-scale traffic generation while improving the accuracy of fine-grained traffic synthesis.

Recently, the emergence of diffusion models has offered promising insights for fine-grained traffic generation. Diffusion models operate by first progressively injecting noise into the original data and subsequently denoising step-by-step to reconstruct high-resolution images from pure noise. This denoising paradigm naturally aligns with the goal of fine-grained mobile traffic synthesis. Inspired by this, we aim to explore a control mechanism for the intermediate states in the noise-adding and denoising processes, as shown in Fig. 2, aligning the variation of noise intensity with the change in spatiotemporal resolution of network traffic. We seek to make the denoising process progressively *zooms in* on the network traffic, revealing increasingly finer spatiotemporal details at each step.

However, achieving this goal presents two main challenges. First, it remains unclear how to design effective denoising procedures within the diffusion framework to accurately represent multi-scale network traffic. Second, it is challenging to model and preserve the cross-resolution dependencies and statistical constraints between traffic at different granularities.

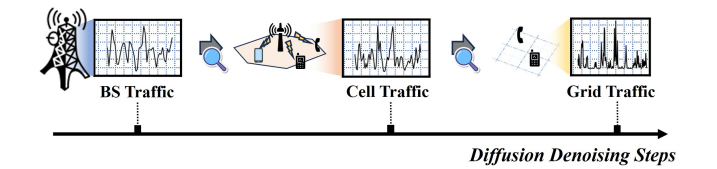


Fig. 2: Align the spatiotemporal refinement relationships of multi-scale network traffic with the denoising process of diffusion models.

To address the above challenges, we propose **ZoomDiff**, a multi-resolution mobile traffic generation model. It achieves a mapping from Urban Environmental Context (UEC) to multilevel network traffic, allowing for a zoom-like progressive generation for traffic with different scales. First, we design Denoising Refinement Diffusion Models (DRDM). It is a multi-stage diffusion framework, enabling controllable denoising intermediates through a Hierarchical Noise-adding Process (HNaP) and a Resolution Refinement Denoising Process (RRDP). Multi-scale traffic with different resolutions can be directly extracted from intermediate states at corresponding diffusion steps. Second, we design a diffusion prior noise mechanism to establish correlations between adjacent noiseadding and denoising stages. This design enables the coarseresolution traffic to serve as guidance to control the generation of high-resolution traffic. Moreover, we discussed the noise scheduling strategies and the Resolution Greediness Preference of the multi-stage model required for implementing DRDM, and revised the corresponding strategies in conventional diffusion models. We found that the combination of discrete noise intensity, discrete noise-adding, and discrete denoising strategies enables ZoomDiff to achieve optimal multi-scale generation performance. The main contributions can be summarized as follows:

- To the best of our knowledge, we propose the first unified model capable of simultaneous generation of multi-scale mobile traffic. Leveraging the sophisticated design of DRDM, it aligns the progressive refinement of spatiotemporal scales of network traffic with the denoising process. In other words, multiple intermediate states of the denoising process are constrained to correspond to multi-scale network traffic.
- We design a prior noise guidance mechanism to establish correlations between noise data at different spatiotemporal resolutions, allowing the high-resolution traffic generation to fully leverage the coarse-grained spatiotemporal patterns learned during the generation of lower-resolution traffic.
- Evaluations on real-world datasets demonstrate that the multi-scale traffic generation based on ZoomDiff outperforms state-of-the-art specialized traffic generation models and spatiotemporal generation models. ZoomDiff achieves an average improvement of 18.4% over the second-best model.

ZoomDiff provides an innovative approach to enhancing multi-scale mobile data management through generative Arti-

ficial Intelligence (AI). We further validate that ZoomDiff has excellent performance in the management of traffic refinement and cross-city generalization. This will help construct an effective data platform for joint planning of multi-level mobile networks.

II. RELATED WORK

A. Network Traffic Generation

Mobile traffic generation aims to learn the environmentaware spatiotemporal dynamics by mining the correlation between network traffic and external conditions. Traditional generative algorithms, including mathematical statistics [28], [29] and simulation-based approaches [30]-[32], have limited generalization capabilities. With the development of Machine Learning (ML), generative models such as Generative Adversarial Networks (GANs) [12], [33]-[35] and Transformers [36], [37] can capture the complex correlations between network demand and environmental features in a data-driven manner. Pandey et al. [33] and Li et al. [34] employed GANs to autoregressively model the temporal dynamics of traffic sequences for synthetic traffic generation. Hui et al. [35] integrated urban environments into Urban Knowledge Graphs (UKGs) for generation guidance. As the stable generative capabilities of diffusion models are validated, recent works have attempted to replace GANs with diffusion-based generators. Zhou et al. [38] applied UKG to the diffusion denoising process for accurate urban population generation. Sivaroopan et al. [39] and Jiang et al. [40] converted one-dimensional network traffic into two-dimensional images to leverage the strong image generation capabilities of diffusion models.

However, existing research primarily focuses on traffic generation at a single spatiotemporal resolution. For the task of generating multi-scale traffic, multiple models or separate generations are typically required. In addition, these models are designed for coarse-scale traffic such as BS or cell levels, and perform poorly when generating fine-grained traffic at small grid scales. In contrast, ZoomDiff can generate multi-scale mobile traffic in a single process and progressively guide the generation of fine-grained traffic through coarse-scale traffic, achieving both improved generation accuracy and enhanced efficiency.

B. Generative Management of Mobile Data

Generative management of mobile data leverages advances in generative AI to synthesize, augment, and anonymize datasets such as network traffic [41]–[43] and mobile trajectories [44]–[48], addressing issues of limited data availability and privacy concerns [49]. Traditional simulation [50], [51] or rule-based models [48] often struggled to capture the complex spatiotemporal patterns inherent in mobile data, whereas modern deep generative models such as GANs and diffusion models learn these patterns directly from real data, producing high-fidelity synthetic data that preserve key statistical properties of the original. Thirumuruganathan *et al.* [52] trained deep generative models to learn the underlying data

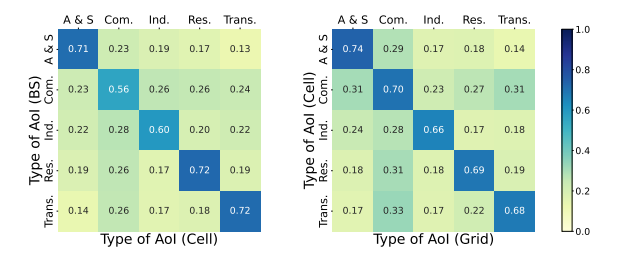


Fig. 3: Heatmaps of RV-coefficients between different levels of traffic across various AoI types.

distribution with high fidelity for approximate query processing in databases. Li *et al.* [41] proposed IoTGemini, a two-module framework with a Packet-Sequence GAN to generate realistic IoT network traffic. In the realm of human mobility, Zhang *et al.* [44] use a clustering-based sequence GAN to capture diverse movement modalities and generate synthetic user trajectories that closely emulate real-world travel patterns. These generative AI methods enable scalable data augmentation and privacy-preserving data sharing in mobile computing. [49] highlights that generative approaches not only enhance the realism of synthetic mobile data but also outperform conventional methods in retaining essential spatiotemporal characteristics, thereby significantly advancing mobile data management in terms of fidelity and utility.

III. PRELIMINARY

In this section, we first qualitatively validate the spatiotemporal correlations across different scales of mobile traffic. Then, the formulation of the canonical diffusion models is briefly outlined. Finally, we present a problem definition for multi-scale mobile traffic generation.

A. Correlations among Multi-scale Network Traffic

The network traffic across different scales, including the BS traffic, cell traffic, and grid-level traffic, exhibits a top-down aggregation relationship due to the inherent hierarchy among their service areas. Figure 4 shows the temporal decomposition of hourly BS traffic, cell traffic, and 50m grid traffic from three kinds of Area of Interest (AoI) over one week. The trend component reflects the distribution of daily average traffic over seven days, while the seasonal component captures the temporal patterns of daily traffic after removing the trend. To be quantitative, Fig. 3 computes the RV-coefficients [53] between adjacent levels of network traffic. It can be observed that traffic at neighboring scales within the same AOI exhibits high similarity. This provides the theoretical foundation for jointly generating multi-scale traffic, where coarse-grained traffic can guide the generation of fine-grained traffic. The RV-coefficient is defined as:

$$\mathcal{R}(\Gamma_1, \Gamma_2) = \frac{\text{tr}(\Gamma_1 \Gamma_1^{\intercal} \Gamma_2 \Gamma_2^{\intercal})}{\sqrt{\text{tr}((\Gamma_1 \Gamma_1^{\intercal})^2) \cdot \text{tr}((\Gamma_2 \Gamma_2^{\intercal})^2)}}, \tag{1}$$

which is used to measure the similarity between multidimensional data matrices. Γ_1 and Γ_2 denote two high-dimensional data matrices, and tr computes the trace of a matrix.

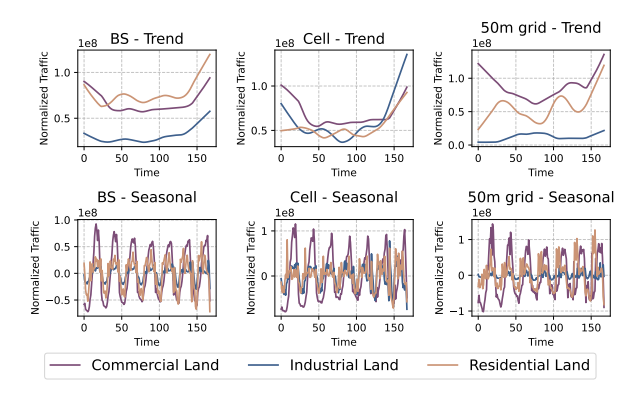


Fig. 4: Time series decomposition of BS, Cell, and 50m grid traffic.

B. Problem Formulation

Mobile network traffic at different layers of network nodes reflects user demand distributions at different spatiotemporal scales. Given the UEC c, the objective of the model is to learn a mapping from UEC to the corresponding regional mobile traffic x, and simultaneously generate multi-level traffic within the region at different spatiotemporal resolutions. Consider a mobile network with $K \geq 2$ levels, let $x_{s_{\delta_k}t_{\tau_k}}$ denote the mobile traffic at level k with spatial resolution s_{δ_k} and temporal resolution t_{τ_k} , where $1 \leq k \leq K$, $\delta_k \geq \delta_{k-1}$ and $\tau_k \geq \tau_{k-1}$. This mapping can be expressed as $c \mapsto (x_{s_{\delta_1}t_{\tau_1}}, ..., x_{s_{\delta_{K-1}}t_{\tau_{K-1}}}, x_{s_{\delta_K}t_{\tau_K}})^{T \times H \times W}$, where T denotes the temporal length of the finest traffic series, and H, W represent the finest spatial dimensions. As the spatiotemporal resolution increases, the traffic becomes increasingly influenced by fine-grained urban environments and user behavioral characteristics. Therefore, generating high-dimensional spatiotemporal traffic at fine resolutions is a complex task.

This multi-level traffic generation problem can be abstracted as a conditional generation problem of multi-resolution spatiotemporal sequences. Given the environmental condition c, the K-stage multi-resolution generation problem can be formulated as:

$$(\boldsymbol{x}_{s_{\delta_{1}}t_{\tau_{1}}},...,\boldsymbol{x}_{s_{\delta_{K-1}}t_{\tau_{K-1}}},\boldsymbol{x}_{s_{\delta_{K}}t_{\tau_{K}}}) = \boldsymbol{\Psi}(\boldsymbol{c},K),$$
 (2)

where Ψ denotes the generative model that performs unified modeling and generation of traffic data across all resolutions.

C. Canonical Diffusion Models

The core idea of canonical diffusion models [54]–[56] is to construct a forward diffusion process that gradually perturbs the original data into Gaussian noise, while simultaneously training a learnable reverse denoising process to recover the original data. According to Ho *et al.* [54], the forward diffusion process can be obtained as:

$$\boldsymbol{x}^{(n)} = \sqrt{\alpha^{(n)}} \boldsymbol{x}^{(0)} + \sqrt{1 - \alpha^{(n)}} \boldsymbol{\epsilon}, \quad \boldsymbol{\epsilon} \sim \mathcal{N}(0, \boldsymbol{I}),$$
 (3)

where n is the order of diffusion steps, $\boldsymbol{x}^{(n)}$ is the noised sample at step n, $\alpha^{(n)} = \prod_{i=1}^n \hat{\alpha}_i$ is a predefined noise scheduling coefficient that controls the noise intensity at each step. After

a sufficient number of steps N, the data distribution converges toward a standard normal distribution $\boldsymbol{x}^{(N-1)} = \boldsymbol{\epsilon} \sim \mathcal{N}(0, \boldsymbol{I})$.

During the forward process, the diffusion model learns a parameterized neural network $\epsilon_{\theta}(\boldsymbol{x}^{(n)}, n)$ to approximate the noise added in each step. θ means the model parameters. The training objective is typically formulated as a mean-squared error loss for noise reconstruction:

$$\mathcal{L}_{S} = \mathbb{E}_{\boldsymbol{x}^{(0)}, \boldsymbol{\epsilon}, n} \left[\left\| \boldsymbol{\epsilon}_{\theta}(\boldsymbol{x}^{(n)}, n) - \boldsymbol{\epsilon} \right\|_{2}^{2} \right]. \tag{4}$$

In the reverse process, the model denoises from a standard Gaussian noise $x^{(N-1)} = \epsilon$ and performs iterative reverse sampling according to [54]:

$$\boldsymbol{x}^{(n-1)} = \frac{1}{\sqrt{\hat{\alpha}^{(n)}}} \left(\boldsymbol{x}^{(n)} - \frac{1 - \hat{\alpha}^{(n)}}{\sqrt{1 - \alpha^{(n)}}} \boldsymbol{\epsilon}_{\theta}(\boldsymbol{x}^{(n)}, n) \right) + \sigma^{(n)} \boldsymbol{\epsilon}, \quad (5)$$

where
$$\sigma^{(n)} = \sqrt{1 - \hat{\alpha}^{(n-1)}} (1 - \alpha^{(n-1)}) / (1 - \alpha^{(n)}).$$

Limitation. Canonical diffusion models are fundamentally designed for *single-resolution* data generation. That is, they progressively denoise random noise at a fixed resolution throughout the diffusion process. However, the intermediate states during denoising are typically unstructured and semantically meaningless, offering no interpretable representation of coarser or finer information. Moreover, the models lack mechanisms to model dependencies across different spatiotemporal resolutions, treating each step as an isolated transformation. As a result, canonical diffusion frameworks are inherently limited in addressing the requirements of the multi-resolution mobile traffic generation problem.

D. Technical Challenges

To address the problem of multi-scale mobile traffic generation, it is necessary to design a novel diffusion model architecture that goes beyond the limitations of canonical frameworks. However, this design process still faces the following three key challenges:

- How to leverage diffusion models to construct a generative framework for multi-resolution spatiotemporal data;
- How to enable the model to understand the intrinsic relationships among multi-resolution data;
- How to equip the model with the ability to capture spatiotemporal dependencies in high-dimensional traffic sequences.

IV. METHOD

To address the technical challenges, we propose ZoomDiff, a diffusion-based model for multi-resolution mobile traffic generation. ZoomDiff restructures the intermediate states of the denoising process so that they are no longer disordered noisy data, but rather a series of data representations with progressively increasing resolution throughout the denoising trajectory. In other words, it introduces a customized denoising process that gradually zooms in on finer details of regional mobile traffic. Fig. 5 shows the overall framework of ZoomDiff. It consists of two components: the Environment-aware Conditional Information and the DRDM. DRDM takes a series of conditions that are aligned with the spatiotemporal

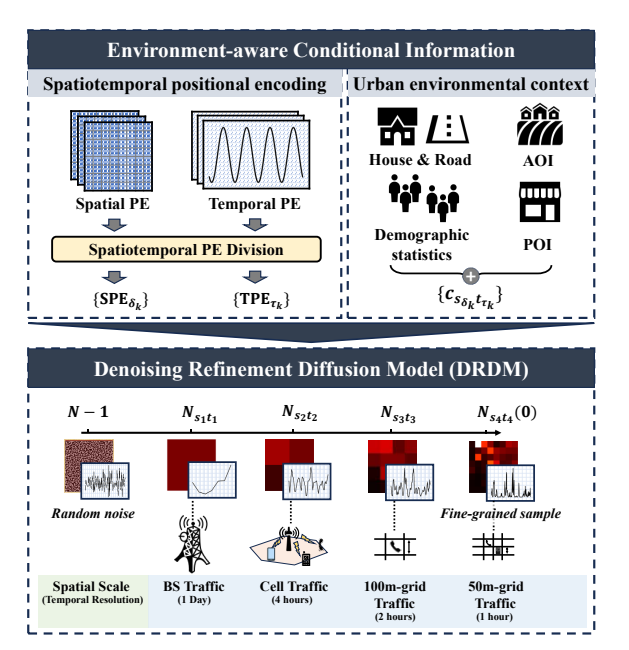


Fig. 5: Overall framework of ZoomDiff. It consists of two components: the Environment-aware Conditional Information and the Denoising Refinement Diffusion Models (DRDM).

resolutions of the network scales as input. It outputs multiscale mobile traffic with various spatiotemporal resolutions through different intermediate denoising states, and ultimately produces a fine-grained sample corresponding to the smallest spatial scale and the finest temporal resolution.

A. Environment-aware Conditional Information

The environment-aware conditional information consists of the Spatiotemporal Positional Encoding (StPE) and the UEC. The StPE is designed to enable the diffusion model to capture temporal characteristics and spatial relationships in high-dimensional traffic data. The UEC is derived from multidimensional urban data, which is relevant to mobile users' traffic demands.

1) Spatiotemporal Positional Encoding (StPE): StPE is composed of a Temporal Positional Encoding (TPE) and a Spatial Positional Encoding (SPE). The TPE is constructed using a 128-D sinusoidal encoding, which is formulated as

TPE(t) =
$$\left[\sin \left(t/10000^{\frac{2i}{128}} \right), \cos \left(t/10000^{\frac{2i}{128}} \right) \right]_{i=0}^{63}$$
, (6)

and the SPE is implemented as a 128-D learnable embedding, which can be represented as SPE $\in \mathbb{R}^{128 \times H \times W}$. Different SPEs are used for different spatial resolutions. TPE and SPE are concatenated to form a high-dimensional StPE: $[\text{TPE}, \text{SPE}]^{256 \times L \times H \times W}$. This encoding is further coarsened via a downsampling-based Spatiotemporal PE Division to align with the multi-resolution traffic, yielding encoding series $\{\text{TPE}_{\tau_k}\}$ and $\{\text{SPE}_{\delta_k}\}$. They help ZoomDiff to understand various spatiotemporal relations across resolutions. The formulations of TPE and SPE are given as follows.

2) Urban Environment Context (UEC): Considering generality and accessibility, we construct the UEC using the following four types of urban data: House & Road type $c_S \in \mathbb{N}^{H imes W}$ AOI types $c_{AoI} \in \mathbb{N}^{H \times W}$, POI embedding $c_{PoI} \in \mathbb{N}^{d \times H \times W}$, and historical demographic statistics $c_{\mathsf{pop}} \in \mathbb{N}^{T \times H \times W}$. $c_S \in$ $\mathbb{N}^{H \times W}$ indicates information about indoor and outdoor areas as well as road types; $c_{\text{AoI}} \in \mathbb{N}^{H \times W}$ represent the functional zoning of different urban areas; $c_{\text{PoI}} \in \mathbb{N}^{d \times H \times W}$ reflects the types and quantity distribution of urban entities surrounding a region. $c_{\text{pop}} \in \mathbb{N}^{T \times H \times W}$ represents the historical statistical distribution of the regional population. To obtain a unified representation, we use a set of MLP-based mappers $\{f_i\}_{i=1}^4$ to project the above data into the same latent space. They are then combined to obtain high-resolution urban environment semantics: $c = f_1(c_S) \oplus f_2(c_{AoI}) \oplus f_3(c_{PoI}) \oplus f_4(c_{pop})$. We further decompose c into a series of UEC $\{c_{s_{\delta_k}t_{\tau_k}}\}$ aligned with the target spatiotemporal resolutions through downsampling. It could guide the conditional distribution fitting at each stage of the DRDM.

B. Denoising Refinement Diffusion Models (DRDM)

DRDM is a multi-resolution diffusion model architecture. The denoising process of DRDM is shown in Fig. 6. It restructures the intermediate states of the denoising process, allowing a single denoising trajectory to generate samples with varying spatiotemporal resolutions at different nodes. The multi-resolution data generation capability of DRDM is achieved through a customized multi-stage forward and reverse process, including the HNaP and the RRDP. DRDM uses a customized denoising network to estimate noise from multidimensional conditions. It further incorporates a noise prior guidance mechanism to establish connections across stages with different spatiotemporal resolutions. This section provides a detailed introduction to the noise prior guidance mechanism, HNaP, and RRDP, and discusses specialized noise scheduling and Resolution Greediness Preference strategies adapted for DRDM.

1) Diffusion Noise Prior Guidance: In Section III-C, Eq. 3 presents the general form of the forward process in diffusion models. Inspired by [57], suppose the real data $\boldsymbol{x}^{(0)}$ contains a fixed, prior-known component \boldsymbol{H} , such that $\boldsymbol{x}^{(0)} = \boldsymbol{H} + \Delta \boldsymbol{x}^{(0)}$, where $\Delta \boldsymbol{x}^{(0)}$ denotes the residual between $\boldsymbol{x}^{(0)}$ and \boldsymbol{H} . Then, Eq. 3 can be rewritten as:

$$\boldsymbol{x}^{(n)} = \sqrt{\alpha^{(n)}} \underbrace{(\boldsymbol{H} + \Delta \boldsymbol{x}^{(0)})}_{\boldsymbol{x}^{(0)}} + \sqrt{1 - \alpha^{(n)}} \boldsymbol{\epsilon}. \tag{7}$$

By equivalently transforming the above equation, we obtain:

$$\epsilon = \frac{\boldsymbol{x}^{(n)} - \sqrt{\alpha^{(n)}}(\boldsymbol{H} + \Delta \boldsymbol{x}^{(0)})}{\sqrt{1 - \alpha^{(n)}}}$$

$$= \underbrace{\frac{\boldsymbol{x}^{(n)} - \sqrt{\alpha^{(n)}}\Delta \boldsymbol{x}^{(0)}}{\sqrt{1 - \alpha^{(n)}}}}_{\Delta \epsilon} - \underbrace{\frac{\sqrt{\alpha^{(n)}}\boldsymbol{H}}{\sqrt{1 - \alpha^{(n)}}}}_{\hat{\epsilon}}$$

$$:= \Delta \epsilon - \hat{\epsilon}$$
(8)

where $\hat{\epsilon}$ is defined as the prior noise component associated with the fixed part H. The model's learning objective is to fit

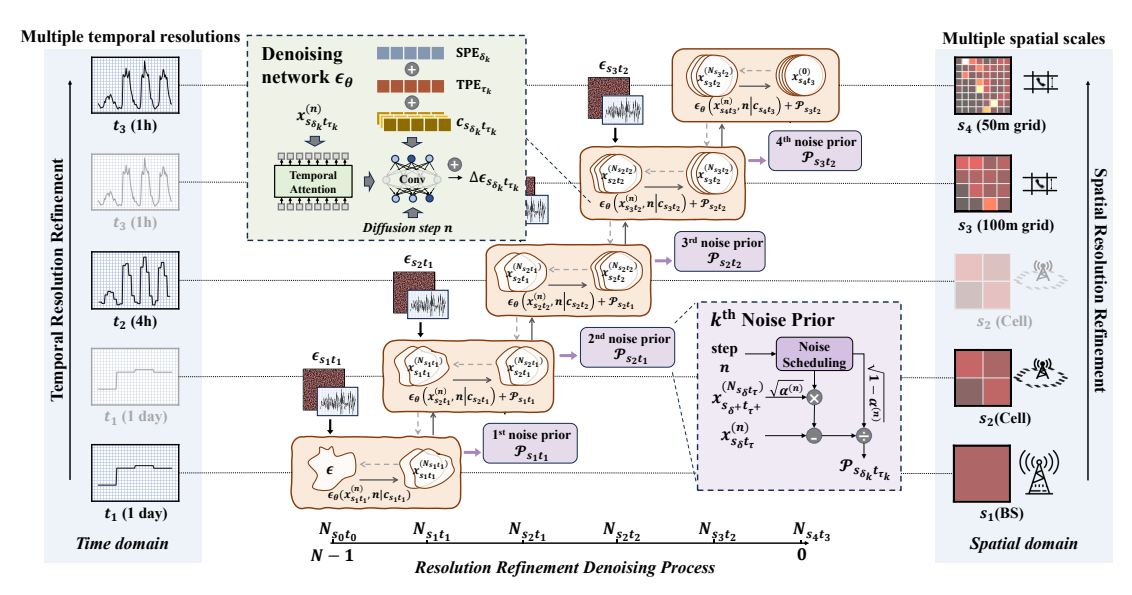


Fig. 6: The pipeline of the multi-stage denoising process of DRDM. Different stages correspond to different spatial scales and temporal resolutions, where the gray color indicates that the spatial scale or temporal resolution at that stage remains unchanged compared to the previous stage.

the residual noise $\Delta \epsilon = \epsilon + \hat{\epsilon}$. The prior noise mechanism introduces prior knowledge into both the noise-adding and denoising processes, enabling the diffusion model to generate data biased toward a given prior distribution. The loss function of the diffusion model with the applied prior noise mechanism in the forward process can be formulated as:

$$\mathcal{L}_{\mathbf{m}} = \mathbb{E}_{\boldsymbol{x}^{(0)}, \boldsymbol{\epsilon}, n} \left[\left\| \boldsymbol{\epsilon}_{\boldsymbol{\theta}}(\boldsymbol{x}^{(n)}, n) - (\boldsymbol{\epsilon} + \hat{\boldsymbol{\epsilon}}) \right\|_{2}^{2} \right], \tag{9}$$

where the objective of the denoising network $\epsilon_{\theta}(\boldsymbol{x}^{(n)}, n)$ is to approximate the noise residual $\Delta \epsilon$.

2) Hierarchical Noise-adding Process: To enable the reduction of intermediate states in the denoising process, we first introduce a customized design for the noise-adding process in DRDM. Given a K-level ordered sequence tuple with progressively refined resolutions $\{\boldsymbol{x}\}_K = \{\boldsymbol{x}_{s_1t_1},...,\boldsymbol{x}_{s_{\delta_K-1}t_{\tau_{K-1}}},\boldsymbol{x}_{s_{\delta_K}t_{\tau_K}}\}$, where $\boldsymbol{x}_{s_{\delta_K}t_{\tau_K}}$ has the highest spatiotemporal resolution and serves as the starting point of noise addition. Unlike the forward process in canonical diffusion models, HNaP is a multi-stage diffusion process. The total number of diffusion steps N is divided into multiple segments corresponding to the resolution levels in $\{\boldsymbol{x}\}_K$. These segment boundaries are denoted by $\{N\}_K = \{N_{s_{\delta_K}t_{\tau_K}}(=0), N_{s_{\delta_{K-1}}t_{\tau_{K-1}}},...,N_{s_1t_1}\}$, with $N_{s_0t_0} = N$. During the k-th noise-adding sub-process in HNaP,

During the k-th noise-adding sub-process in HNaP, where $k \in \{1,2,...,K\}$, the diffusion step $n \in [N_{s_{\delta_k}t_{\tau_k}},N_{s_{\delta_{k-1}}t_{\tau_{k-1}}})$. This sub-process takes $\boldsymbol{x}_{s_{\delta_k}t_{\tau_k}}$ as the initial state for noise addition. After iterating through all k, HNaP constructs a trajectory starting from $\boldsymbol{x}_{s_{\delta_k}t_{\tau_k}}$ and ending at $\boldsymbol{\epsilon} \sim \mathcal{N}(0,\boldsymbol{I})$, with intermediate states representing data at various spatiotemporal resolutions. To associate successive stages, we adopt a diffusion prior mechanism. In the k-th noise-adding sub-process, we treat $\boldsymbol{x}_{s_{\delta_{k+1}}t_{\tau_{k+1}}}$ as a prior bias

and define the k^{th} prior noise as

$$\mathcal{P}_{s_{\delta_{k-1}}t_{\tau_{k-1}}} = \begin{cases} \frac{\sqrt{\alpha_k^{(n)}} \mathbf{z}_{s_{\delta_{k-1}}t_{\tau_{k-1}}}}{\sqrt{1-\alpha_k^{(n)}}}, & \text{if } k > 1\\ 0, & \text{if } k = 1 \end{cases}$$
 (10)

Then, HNaP can be formally formulated as

$$\boldsymbol{x}_{s_{\delta_k}t_{\tau_k}}^{(n)} = \sqrt{\alpha_k^{(n)}} \boldsymbol{x}_{s_{\delta_k}t_{\tau_k}}^{(0)} + \sqrt{1 - \alpha_k^{(n)}} (\boldsymbol{\epsilon} + \mathcal{P}_{s_{\delta_{k-1}}t_{\tau_{k-1}}}). \quad (11)$$

Under this formulation, the training objective becomes a diffusion-prior-based loss:

$$\mathcal{L}_{\text{HNap}} = \mathbb{E}_{\boldsymbol{x}_{s_{\delta_{k}}t_{\tau_{k}}}, \epsilon, n} \left[\left\| \left(\boldsymbol{\epsilon}_{\theta}(\boldsymbol{x}_{s_{\delta_{k}}t_{\tau_{k}}}^{(n)}, n | \boldsymbol{c}_{s_{\delta_{k}}t_{\tau_{k}}} \right) + \mathcal{P}_{s_{\delta_{k-1}}t_{\tau_{k-1}}} \right) - \boldsymbol{\epsilon} \right\|_{2}^{2} \right]. \tag{12}$$

In HNaP, the step segmentation method $\{N\}_K$ is a mapping over k, which we refer to as Resolution Greediness Preference (RGP) in Multi-stage Denoising; similarly, the noise coefficient $\alpha_k^{(n)}$ is also a mapping over k, referred to as Noise Scheduling. In Section IV-C and Section IV-D, we provide a detailed discussion and analysis of different noise scheduling strategies and diffusion step distributions.

3) Resolution Refinement Denoising Process: HNaP provides K-1 controllable intermediate states with progressively coarsened spatiotemporal resolutions for the forward process of DRDM. Since the noise-adding and denoising processes in diffusion models are symmetric, the reverse process of DRDM also contains K-1 controllable intermediate states, but with gradually refined spatiotemporal resolutions. We refer to this process as the RRDP. Similar to Eq. 5, RRDP can be formally expressed as:

$$\boldsymbol{x}_{s_{\delta_{k}}t_{\tau_{k}}}^{(n-1)} = \frac{1}{\sqrt{\alpha_{k}^{(n)}}} \left(\boldsymbol{x}_{s_{\delta_{k}}t_{\tau_{k}}}^{(n)} - \frac{1 - \alpha_{k}^{(n)}}{\sqrt{1 - \bar{\alpha}_{k}^{(n)}}} \Sigma_{k} \right) + \sigma_{k}^{(n)} \boldsymbol{\epsilon}, \quad (13)$$

where $\epsilon \sim \mathcal{N}(0, \boldsymbol{I}), \; \Sigma_k = \epsilon_{\theta}(\boldsymbol{x}_{s\delta_k t \tau_k}^{(n)}, n) + \mathcal{P}_{s\delta_{k-1} t \tau_{k-1}},$ and $\sigma_k^{(n)} = \sqrt{1 - \hat{\alpha}_k^{(n-1)}} (1 - \alpha_k^{(n-1)})/(1 - \alpha_k^{(n)})$. During the execution of the reverse process, n is iterated backward from N-1 to 0, while k increases step by step from 1 to K according to the value of n. The prior noise $\mathcal{P}_{s\delta_k t \tau_k}$ can be computed from the denoised sample at the adjacent stage $\boldsymbol{x}_{s\delta_k t \tau_k}^{N_{s\delta_k t \tau_k}}$. Based on the above process, RRDP allows us to directly extract K denoised outputs with different spatiotemporal resolutions at steps $n = N_{s_1 t_1}, \ldots, N_{s\delta_{K-1} t \tau_{K-1}}, N_{s\delta_K t \tau_K}(0)$.

4) Denoising Network: The denoising network is the core component of a diffusion model responsible for progressively restoring the data distribution structure from noisy samples. As shown in Fig. 6, DRDM shares the same denoising network ϵ_{θ} across all stages, while controlling it with inputs of different spatiotemporal scales to estimate noise at each stage. It maps the noisy data $\boldsymbol{x}_{s_{\delta_{L}}t_{\tau_{L}}}$, the UEC (including $TPE_{\tau_{k}}$, $SPE_{\delta_{k}}$, and $\boldsymbol{c}_{s_{\delta_k}t_{\tau_k}}$), and the diffusion step n into a unified embedding space through convolutional layers. These embeddings are then fused by element-wise addition. The convolutional layers also act as noise fitters, mapping the fused embeddings at the output layer to the estimated noise residual $\Delta \epsilon_{s_{\delta_{t}}t_{\tau_{t}}}$. The inclusion of conditional terms enables the denoising network to estimate the conditional noise distribution under specific external conditions $\boldsymbol{c}_{s_{\delta_k}t_{\tau_k}}$, expressed as $\epsilon_{\theta}(\boldsymbol{x}_{s_{\delta_k}t_{\tau_k}}^{(n)}, n|\boldsymbol{c}_{s_{\delta_k}t_{\tau_k}})$. We add $\Delta \boldsymbol{\epsilon}_{s_{\delta_k}t_{\tau_k}}$ to the prior noise $\mathcal{P}_{s_{\delta_{k-1}}t_{\tau_{k-1}}}$ and train the denoising network within HNaP using Eq. (12). RRDP employs the trained denoising network to recover the original data from random noise through Eq. (13).

C. Noise Scheduling for DRDM

Noise scheduling is a mechanism in diffusion models that defines how noise intensity varies over time between the forward and reverse processes. Canonical diffusion models typically adopt a continuous linear schedule, where the noise strength $\hat{\alpha} \in (0,1)$ increases linearly with n, and the data is progressively and continuously noised according to Eq. 3. However, since DRDM segments the denoising process, traditional noise scheduling strategies may no longer be suitable. To effectively constrain the intermediate states of the denoising process, we explore different noise scheduling strategies from three aspects: noise intensity, noise-adding scheme, and denoising scheme. The noise scheduling of the forward noise-adding process is illustrated in Fig. 7, while the scheduling of the reverse denoising process is shown in Fig. 8.

1) Noise intensity schedules: We define two types of noise intensity schedules: Continuous Noise (CN) and Segmented Noise (SN). CN corresponds to the monotonic noise intensity used in canonical diffusion models. The noise strength $\hat{\alpha}$ varies continuously from 0 to 1 across all timesteps:

$$\alpha_{\text{CN}}^{(n)} = n/N. \tag{14}$$

In DRDM, we need to constrain the intermediate states at different stage nodes of the denoising process to represent network traffic with specific spatiotemporal scales. The conventional CN causes all diffusion steps, except for the initial

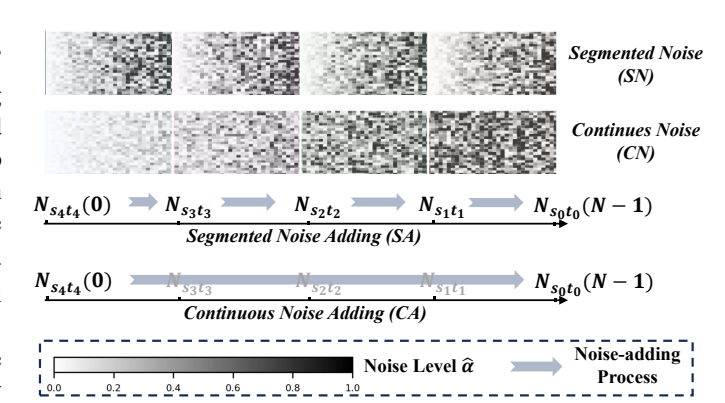


Fig. 7: Noise scheduling for DRDM in the noise-adding process.

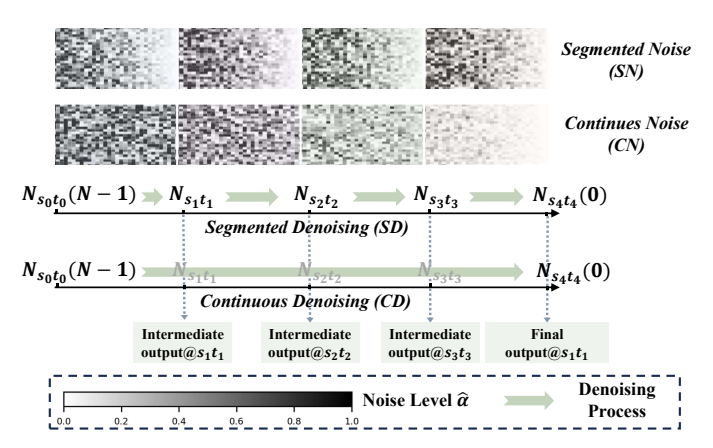


Fig. 8: Noise scheduling for DRDM in the denoising process.

noise-adding point, to contain a certain level of random noise, leading to a deviation between the intermediate states at these nodes and the distributions of traffic at corresponding scales. To address this issue, we propose SN. It linearly schedules $\hat{\alpha}$ within each stage while maintaining overall continuity in (0,1):

$$\alpha_{\text{SN}}^{(n)} = (n - N_{s_{\delta_k} t_{\tau_k}}) / (N_{s_{\delta_{k-1}} t_{\tau_{k-1}}} - N_{s_{\delta_k} t_{\tau_k}}), \quad (15)$$

where $n \in [N_{s_{\delta_k}t_{\tau_k}}, N_{s_{\delta_{k-1}}t_{\tau_{k-1}}}]$, $k=1,2,\ldots,K$. This strategy ensures that the noise intensity at each intermediate node of the RRDP is zero, allowing noise-free traffic sequences with specific scales to be extracted at the corresponding nodes during the denoising process.

2) Noise adding schedules: We define two types of noise adding schedules: Segmented Noise Adding (SA) and Continuous Noise Adding (CA). SA and CA are independent of the noise intensity scheduling strategy, and their difference lies in whether the starting point of noise addition changes at each stage during the forward process. The CA strategy is consistent with canonical diffusion models, as shown in Eq. (3). Its noise-adding starting point always remains the data at diffusion step 0, i.e., in Eq. (11), $\mathbf{x}_{s\delta_k t_{\tau_k}}^{(0)} = \mathbf{x}_{s\delta_K t_{\tau_K}}^{(0)} = \mathbf{x}_{s\delta_K t_{\tau_K}}^{(0)} = \mathbf{x}_{s\delta_K t_{\tau_K}}^{(0)} = \mathbf{x}_{s\delta_K t_{\tau_K}}^{(0)}$

$$\alpha_{k,CA}^{(n)} = \alpha^{(n)}, \ \alpha^{(n)} \in \{\alpha_{CN}^{(n)}, \alpha_{SN}^{(n)}\}.$$
 (16)

To effectively constrain the intermediate states during the denoising process, we explicitly provide samples at the stage nodes of the noise-adding process. As shown in Fig. 7, the SA strategy adopts segmented noise addition. Suppose our target is to generate network traffic at four spatiotemporal scales s_1t_1 , s_2t_2 , s_3t_3 , s_4t_4 , ranging from coarse to fine, where s_4 represents the smallest spatial scale and t_4 denotes the finest temporal resolution. In HNaP, the prior known multilevel network traffic $\boldsymbol{x}_{s_4t_4}$, $\boldsymbol{x}_{s_3t_3}$, $\boldsymbol{x}_{s_2t_2}$, $\boldsymbol{x}_{s_1t_1}$ are respectively used as the noise-adding starting points for each stage. That is, in Eq. (11), $\boldsymbol{x}_{s_{b_k}t_{\tau_k}}^{(0)} \neq \boldsymbol{x}^{(0)}$, $k \leq K-1$,

$$\alpha_{k,\mathrm{SA}}^{(n)} = \alpha^{(n-N_{s_{\delta_{k-1}}t_{\tau_{k-1}}})}, \ \alpha^{(n)} \in \{\alpha_{\mathrm{CN}}^{(n)}, \alpha_{\mathrm{SN}}^{(n)}\}. \eqno(17)$$

3) Denoising schedules: Corresponding to the noise adding schedules, we define two types of denoising schedules: Segmented Denoising (SD) and Continuous Denoising (CD). The CD strategy is consistent with canonical diffusion models. For $n \in \{N-1, N-2, ..., 1\}$, the denoising starting point is the Gaussian random noise ϵ at n = N-1. The SD strategy is a specialized denoising design that works in conjunction with SN. As illustrated in Fig. (8), it sets an independent denoising starting point (random noise) for each denoising stage, and each stage individually performs a denoising sub-process from noise to data at the corresponding scale. It is important to note that this is not a cascade of multiple diffusion models, since all stages share the same denoising network ϵ_{θ} .

D. Resolution Greediness Preference in Multi-stage Denoising

Resolution Greediness Preference (RGP) refers to the segmentation strategy of the noise-adding and denoising processes. The variation in final generation accuracy under different RGPs reflects the relative importance of precision across resolution stages. We propose three types of RGP as follows:

- *Uniform scheduling*: As shown in Fig. 9(a), the diffusion steps are evenly allocated across different spatial scales and temporal resolutions, respectively;
- Coarse-grained greedy scheduling (Coarse Gr.): As shown in Fig. 9(a), the number of stages K equals the larger of the temporal resolutions and spatial scales. The stages corresponding to the lower spatial or temporal resolution levels are placed toward the later steps of denoising:
- Fine-grained greedy scheduling (Fine Gr.): As shown in Fig. 9(a), the number of stages K equals the larger of the temporal and spatial resolution levels. The stages corresponding to the higher spatial or temporal resolution levels are placed earlier in the denoising process.

V. EVALUATION

To evaluate the performance of ZoomDiff on generating multi-scale mobile network traffic with various resolutions, we conduct experiments on a real-world mobile network traffic dataset collected from Nanning, China, and compare it against 10 state-of-the-art baselines.

A. Experimental Setup

- 1) Dataset: We use a real-world mobile network traffic dataset from Nanning, China, which includes mobile traffic records over one week at four layers: BS, Cell, 100m grid, and 50m grid. Due to the limited accessibility of multi-level traffic data, traffic at the BS, Cell, and 100m grid scales is aggregated from the 50m grid traffic according to their respective coverage areas. The finest temporal resolution is 1 hour. Divided by the Yongjiang River, the dataset is split into a South Bank subdataset and a North Bank sub-dataset. The South Bank subdataset contains 1.4k BSs, 5.7k cells, 23k 100m grids, and 92k 50m grids, while the North Bank subset includes 2.8k BSs, 11k cells, 45k 100m grids, and 182k 50m grids. The dataset is provided by China Mobile.
- 2) Evaluation Metrics: We use four metrics to evaluate the discrepancy between the generated traffic and the ground-truth traffic.

 $\begin{array}{llll} \textit{Mean Absolute Error (MAE)} & \text{measures the difference} \\ \text{between predicted } \hat{\boldsymbol{x}} & \text{and ground truth} & \boldsymbol{x} \colon r_{\text{MAE}} = \\ \frac{1}{T \cdot H \cdot W} \sum_{t=1}^{T} \sum_{i=1}^{H} \sum_{j=1}^{W} |\hat{\boldsymbol{x}}_{t,i,j} - \boldsymbol{x}_{t,i,j}|. \end{array}$

Root Mean Squared Error (RMSE) measures the average magnitude of the difference between prediction and ground truth, which penalizes larger deviations more heavily: $r_{\text{RMSE}} = \sqrt{\frac{1}{T \cdot H \cdot W}} \sum_{t=1}^{T} \sum_{i=1}^{H} \sum_{j=1}^{W} (\hat{\boldsymbol{x}}_{t,i,j} - \boldsymbol{x}_{t,i,j})^2$.

Spatial RMSE (spRMSE) computes RMSE based on time-averaged predictions and ground truths, emphasizing consistency in spatial distribution: $r_{\text{spRMSE}} = \sqrt{\frac{1}{H \cdot W} \sum_{i=1}^{H} \sum_{j=1}^{W} \left(\bar{\hat{\boldsymbol{x}}}_{i,j} - \bar{\boldsymbol{x}}_{i,j}\right)^2}, \text{ where } \bar{\hat{\boldsymbol{x}}}_{i,j} = \frac{1}{T} \sum_{t=1}^{T} \hat{\boldsymbol{x}}_{t,i,j}, \bar{\boldsymbol{x}}_{i,j} = \frac{1}{T} \sum_{t=1}^{T} \boldsymbol{x}_{t,i,j}.$ Peak Signal-to-Noise Ratio (PSNR) evaluates the

Peak Signal-to-Noise Ratio (PSNR) evaluates the reconstruction quality in decibels (dB), using the mean squared error as its basis: $r_{\rm PSNR} = 10 \cdot \log_{10} \left(\frac{L^2}{\rm MSE}\right)$, where L is the maximum possible value of the data.

3) Baselines: We select a total of 10 state-of-the-art baseline models across four categories: i) Basic forecasting models: XGBoost [58] and Transformer [59]; ii) Domain-specific models for network traffic generation: KSTDiff [38], Net-Diffus [39], 5GT-GAN [33], and keGAN [35]; iii) Classic diffusion models: CSDI [55] and DiT [56]; iv) Time series generation models: TimeGAN [60], and Diffusion-TS [61].

B. Overall Performance

In this section, we present the overall performance on generating mobile traffic by ZoomDiff and baselines on the South Bank dataset and the North Bank dataset. We conduct experiments on generating traffic at three spatial scales: BS, 100m grid, and 50m grid. The evaluation results on the South Bank dataset are shown in Table I. The corresponding results on the North Bank dataset are listed in Table II.

According to the results, ZoomDiff performs the best at all resolutions. Compared with the suboptimal model, CSDI, ZoomDiff achieves an average performance improvement of 18.4%. This demonstrates that ZoomDiff effectively captures the spatiotemporal mapping between the urban environment and network demand. An interesting observation is that, as

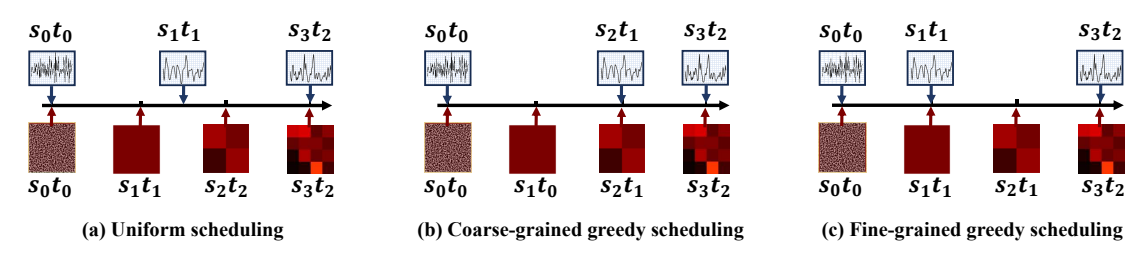


Fig. 9: Three denoising allocation strategies, including the Uniform Strategy, Coarse-grained Greedy Strategy, and Fine-grained Greedy Strategy.

TABLE I: Performance comparison on multi-resolution traffic generation on South Bank, Nanning dataset (**lower is better** for MAE/RMSE/spRMSE, **higher is better** for PSNR). Numbers in parentheses indicate variance. **Bold** numbers indicate the best-performing model for each metric, and <u>underlined</u> numbers indicate the second-best model.

Method	BS traffic		100m grid traffic				50m grid traffic				
	MAE↓ e7(e4)	RMSE↓ e7(e4)	MAE↓ e7(e4)	RMSE↓ e7(e4)	spRMSE↓ e7(e4)	PSNR↑ 1(e-2)	MAE↓ e7(e4)	RMSE↓ e7(e4)	spRMSE↓ e7(e4)	PSNR↑ 1(e-2)	
XGBoost	1.86 (22.7)	2.42 (36.5)	6.31 (54.8)	7.49 (66.2)	6.80 (61.3)	16.1 (7.20)	8.92 (73.5)	8.71 (84.1)	7.97 (76.4)	13.2 (6.70)	
Transformer	2.02 (28.6)	2.41 (41.0)	6.13 (50.1)	7.13 (64.7)	6.71 (58.9)	17.3 (7.90)	7.41 (67.3)	7.07 (72.8)	6.93 (69.5)	14.8 (6.20)	
KSTDiff	1.46 (41.4)	1.92 (47.3)	7.77 (94.3)	12.2 (9.61)	9.21 (11.0)	13.0 (135)	8.76 (13.8)	16.1 (17.2)	11.7 (16.2)	12.9 (13.4)	
NetDiffus	2.36 (48.5)	2.79 (52.2)	78.0 (98.2)	88.4 (103)	87.5 (67.9)	9.02 (3.63)	84.4 (76.1)	95.6 (94.2)	101 (59.0)	8.22 (1.29)	
5GT-GAN	2.63 (5.44)	3.12 (5.48)	4.17 (7.10)	4.97 (6.91)	5.06 (7.09)	18.7 (2.14)	4.50 (8.76)	6.06 (9.84)	6.51 (9.54)	20.8 (2.78)	
keGAN	3.40 (99.1)	4.58 (135)	270 (341)	377 (770)	317 (494)	8.29 (8.08)	377 (231)	472 (631)	422 (335)	6.24 (1.27)	
CSDI	1.18 (41.2)	1.57 (46.8)	2.71 (18.2)	3.92 (22.3)	3.69 (26.8)	26.5 (21.9)	$\frac{3.15}{3.15} (6.76)$ $\underline{3.15} (2.77)$	5.04 (9.00)	4.94 (15.8)	27.6 (22.8)	
DIT	1.34 (28.4)	1.76 (35.2)	2.63 (10.2)	3.89 (26.6)	3.65 (33.1)	26.6 (20.4)		5.26 (4.13)	5.18 (6.03)	28.1 (4.93)	
TimeGAN	7.00 (45.0)	6.76 (50.3)	15.2 (66.0)	17.0 (73.5)	16.1 (71.2)	7.83 (3.20)	26.4 (94.2)	28.7 (102)	27.7 (97.1)	6.60 (2.90)	
Diffusion-TS	1.35 (72.6)	1.73 (77.8)	7.80 (0.125)	8.82 (0.124)	9.27 (0.223)	12.3 (0.350)	7.95 (0.0327)	11.1 (0.0324)	12.1 (0.0807)	14.4 (0.0776)	
ZoomDiff	0.778 (7.86)	1.07 (9.23)	2.17 (10.6)	3.22 (10.1)	2.91 (15.5)	29.1 (9.61)	2.95 (9.05)	4.90 (14.4)	4.72 (16.7)	29.6 (21.3)	

the spatial resolution increases, diffusion models such as CSDI, DiT and ZoomDiff consistently maintain low generation errors, while GAN-based models like keGAN and TimeGAN suffer from significant performance degradation. This is because GANs are more prone to mode collapse when faced with increasingly complex spatiotemporal patterns that increase with spatiotemporal resolution. Diffusion models, on the other hand, benefit from the noise-adding and denoising mechanism, leading to strong robustness. Additionally, the progressive denoising process is similar in effect to multilevel mobile traffic with progressive resolution refinement, validating the rationality of employing diffusion models to design resolution-scalable traffic generators.

C. Multi-resolution Generation

In this section, we compare the denoising intermediate states of CSDI, DiT, and ZoomDiff to validate the effectiveness of our proposed DRDM design. We conduct tests under two resolution configurations:

- **S4T4:** 4 spatial scales (BS, Cell, 100m grid, 50m grid) with 4 temporal resolutions (1 day, 4h, 2h, 1h);
- **S3T4:** 3 spatial scales (Cell, 100m grid, 50m grid) with 4 temporal resolutions (1 day, 4h, 2h, 1h).

We adopt a Fine Gr. RGP, where the number of denoising stages equals the greater resolution levels of the temporal dimension and spatial dimension, and the dimension with fewer levels is aligned to earlier denoising steps. For example,

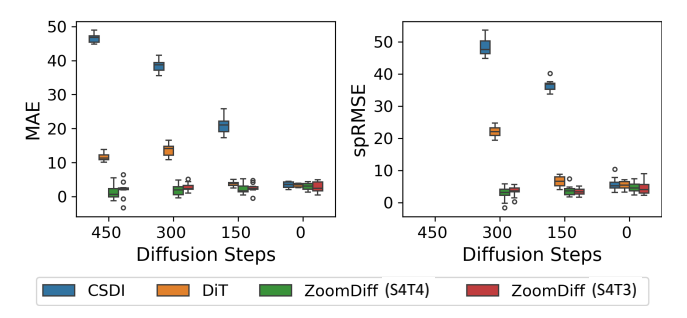


Fig. 10: Performance comparison of intermediate denoising state across different resolution hierarchy settings for CSDI, DiT, and ZoomDiff on the South Bank, Nanning dataset.

under the S3T4 configuration with a total denoising step count of N=600, the stage egment boundarie $\{N_{s_{\delta_k}t_{\tau_k}}\}$ are set at $\{450,300,150\}$. It divides the denoising process into four stages with the following spatiotemporal resolutions: $\{(1 \text{ day, Cell}), (4h, 100\text{m grid}), (2h, 50\text{m grid}), (1h, 50\text{m grid})\}$. For ZoomDiff, we can directly extract the corresponding finegrained data at n=450, 300, 150, and 0.

Fig. 10 provides a performance comparison of intermediate denoising states across different resolution hierarchy settings for CSDI, DiT, and ZoomDiff on the South Bank, Nanning dataset. To intuitively illustrate the designed RRDP for DRDM, Fig. 11 presents the temporal waveforms of intermediate denoising states of CSDI and ZoomDiff (S4T4)

TABLE II: Performance comparison on multi-resolution traffic generation on North Bank, Nanning dataset (**lower is better** for MAE/RMSE/spRMSE, **higher is better** for PSNR). Numbers in parentheses indicate variance. **Bold** numbers indicate the best-performing model for each metric, and underlined numbers indicate the second-best model.

	BS tr	raffic		100m gr	id traffic		50m grid traffic				
Method	MAE↓	RMSE↓	MAE↓	RMSE↓	spRMSE↓	PSNR↑	MAE↓	RMSE↓	spRMSE↓	PSNR↑	
	e7(e4)	e7(e4)	e7(e4)	e7(e4)	e7(e4)	1(e-2)	e7(e4)	e7(e4)	e7(e4)	1(e-2)	
XGBoost	0.960 (22.7)	1.40 (36.5)	4.53 (54.8)	5.60 (66.2)	6.27 (61.3)	20.7 (7.2)	6.55 (73.5)	7.45 (84.1)	7.23 (76.4)	16.9 (6.7)	
Transformer	2.27 (28.6)	2.78 (41.0)	4.57 (50.1)	5.69 (64.7)	6.18 (58.9)	16.1 (7.9)	6.14 (67.3)	7.19 (72.8)	7.64 (69.5)	17.7 (6.2)	
KSTDiff	1.88 (61.8)	2.47 (78.4)	4.55 (89.0)	6.44 (104)	6.08 (144)	23.9 (67.2)	5.51 (34.7)	8.69 (51.9)	8.55 (61.2)	26.4 (34.4)	
NetDiffus	3.40 (32.1)	4.91 (42.3)	21.1 (49.8)	23.9 (63.5)	21.5 (72.0)	10.3 (3.62)	25.3 (43.4)	27.9 (58.0)	32.6 (67.4)	20.5 (2.67)	
5GT-GAN	2.63 (5.44)	3.12 (5.48)	6.53 (3.49)	7.93 (5.00)	7.86 (4.13)	19.1 (0.910)	10.1 (3.23)	12.7 (4.38)	13.0 (4.04)	21.1 (1.19)	
keGAN	5.29 (198)	6.76 (266)	122 (128)	154 (293)	134 (162)	11.1 (3.09)	172 (90.1)	233 (233)	205 (152)	21.5 (4.15)	
CSDI	2.03 (43.6)	2.68 (5.04)	3.36 (22.2)	4.93 (32.3)	4.54 (34.5)	27.8 (19.5)	5.95 (21.5)	7.30 (13.8)	6.50 (12.3)	27.4 (13.2)	
DIT	1.97 (6.32)	2.53 (7.43)	4.29 (25.6)	5.73 (35.1)	5.55 (37.2)	23.5 (13.0)	4.13 (5.17)	6.83 (8.85)	6.75 (11.1)	28.6 (5.10)	
TimeGAN	11.0 (45.0)	12.4 (50.3)	24.2 (66.0)	26.1 (73.5)	25.2 (71.2)	6.76 (3.20)	34.6 (94.2)	37.4 (101)	36.2 (97.1)	7.21 (2.90)	
Diffusion-TS	1.66 (38.3)	2.31 (43.9)	6.88 (1.71)	8.73 (2.07)	8.17 (2.87)	16.9 (0.550)	7.20 (2.12)	10.9 (2.28)	9.64 (4.90)	16.2 (0.390)	
ZoomDiff	0.943 (7.18)	1.21 (9.25)	2.23 (11.6)	3.45 (13.9)	3.01 (12.0)	28.9 (18.8)	3.05 (9.05)	4.99 (19.1)	4.87 (17.4)	28.9 (31.3)	

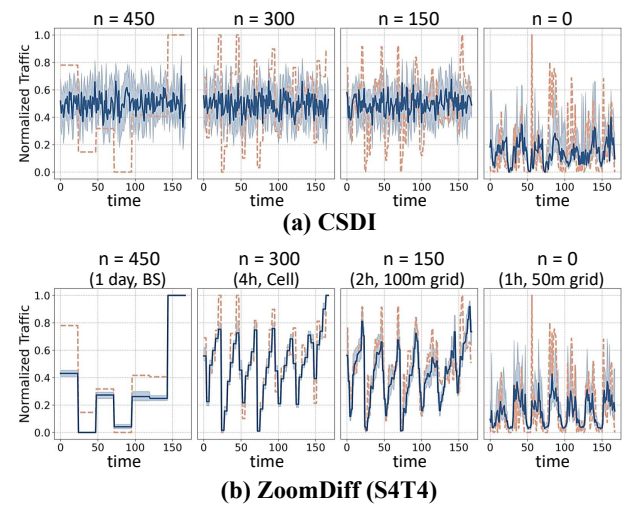


Fig. 11: Traffic series of intermediate denoising states for CSDI and ZoomDiff (S4T4) on the South Bank, Nanning dataset.

extracted at $n=450,\,300,\,150,\,$ and 0. It can be observed that at n=0 (completely denoised), the performances of CSDI, DiT, and ZoomDiff are comparable. However, the intermediate denoising states of CSDI and DiT appear relatively chaotic. In contrast, ZoomDiff is able to produce accurate generation results at different stages of the same denoising process. These intermediate states correspond to network traffic with varying spatio-temporal resolutions, rather than noisy and disordered data.

These findings demonstrate that ZoomDiff can effectively regularize the intermediate states of the denoising process without compromising the final high-resolution generation accuracy, which enables the direct extraction of coarser-resolution network traffic from intermediate states. This design innovatively overcomes the limitation of canonical diffusion models, which can only generate data at a single resolution, and provides a unified paradigm for multi-resolution mobile network traffic generation.

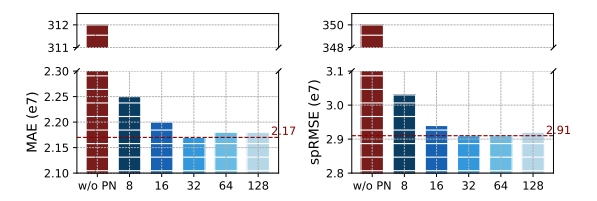


Fig. 12: Ablation Study: Diffusion Prior Noise. w/o PN denotes the removal of prior noise connections between adjacent stages in both the forward and reverse processes. The x-axis values represent the noise dimension D.

D. Ablation Studies

1) Diffusion Noise Prior Guidance: As illustrated in Section IV-B2 and Section IV-B3, we employ a prior noise guidance to allow low-resolution network traffic to guide the generation of high-resolution traffic. To achieve Eq. 11, we use a Multi-Layer Perceptron (MLP) to map the predicted residual noise ϵ and prior noise $\mathcal{P}_{s_{\delta_{k-1}}t_{\tau_{k-1}}}$ in the D-dimensional latent space for concatenation. Fig. 12 shows the impact on high-resolution traffic generation accuracy when removing the prior noise guidance or varying the latent noise dimension D. It can be observed that the prior noise guidance is essential for DRDM, as the limited number of diffusion steps in one stage is insufficient to fully learn the complex spatio-temporal patterns of high-resolution traffic. Increasing the latent dimension of the noise helps the model better disentangle and fuse the spatio-temporal patterns embedded in the random and prior noise. Experiments show that the performance converges when D reaches 32, indicating that further increasing the dimension provides no additional information gain in the noise fusion process.

2) Spatiotemporal Positional Encoding: In this section, we investigate the role of TPE and SPE in helping the model understand the temporal and spatial characteristics of network traffic. We conduct an ablation study targeting this encoding, with the results shown in Fig. 13. The outcome aligns with our

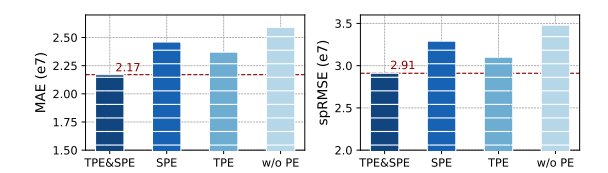


Fig. 13: Ablation Study: Spatiotemporal Positional Encoding. *TPE&SPE* indicates the use of both TPE and SPE, *SPE* indicates the use of SPE only, *TPE* indicates the use of TPE only, and *w/o PE* denotes that neither TPE nor SPE is applied.

expectations: the introduction of both TPE and SPE provides positive gains to the model.

E. Discussion on Schedualing

1) Noise Scheduling: The performance comparison under different noise scheduling is shown in Table III. There are eight possible combinations of noise intensity scheduling, noise adding scheduling, and denoising scheduling. Among them, [CN, CA, CD] corresponds to the scheduling strategy of canonical diffusion models. We tested five strategy combinations listed in Table III. The combination [CN, *, SD] produced good performance for the final output but resulted in collapse when generating intermediate-scale data. This phenomenon also appeared in the traditional strategy [CN, CA, CD], indicating that CN is not suitable for DRDM's multi-stage data generation requirements. The [SN, SA, SD] strategy combination achieved the best performance across all resolutions and serves as the optimal noise scheduling strategy adapted for DRDM. Additionally, schedules with SN enable more accurate low-resolution outputs at intermediate denoising stages. These observations indicate that symmetry between the noise-adding and denoising processes is essential for data recovery, and that segmented noise strength scheduling is needed for DRDM. This is because the reduction of intermediate denoising states cannot be achieved simply by adding or subtracting i.i.d. Gaussian noise.

2) RGP in Multi-stage Denoising: We adopt the S3T2 resolution configuration, and the results are shown in Table IV. The Uniform scheduling divides the denoising process into four stages, while both greedy strategies divide it into three. In terms of the highest-resolution accuracy, the Fine Gr. performs the best, whereas Uniform is relatively less advantageous. This result reflects that, given the same resolution configuration, a smaller number of stages K can lead to more accurate high-resolution generation (with the cost of one fewer observable intermediate denoising state). What's more, sufficient learning of high-resolution spatio-temporal patterns is more critical to achieving high-resolution accuracy than over-emphasizing learning at lower resolutions.

F. Efficiency Analysis

In large-scale mobile data management, efficient modeling and generation of spatiotemporal data are crucial. ZoomDiff enables joint generation of multi-scale mobile traffic, producing network traffic at multiple network layers with different spatial scales and temporal resolutions through a single denoising process of one diffusion model. The time complexity of diffusion models mainly arises from the multi-step denoising process; while traditional diffusion models can only generate data at a single spatiotemporal resolution, ZoomDiff improves the utilization efficiency of the denoising inference process.

To verify the efficiency advantage of ZoomDiff, we conduct a four-level network traffic generation task (BS, cell, 100m grid, 50m grid) for an area containing 500 BSs, including both pre-training and inference. For simplicity, the temporal resolution of traffic at each level is fixed at 1 hour. The batch size is set to 4, and a single NVIDIA A100 GPU is used. Table V presents the comparison results between ZoomDiff and representative diffusion models (CSDI, DIT) in terms of parameter scale, training speed, and inference speed. It can be observed that ZoomDiff, while maintaining a small number of parameters (0.504M), achieves remarkable acceleration performance. Its training time is reduced from 22.9 s/epoch in CSDI to 12.25 s/epoch, representing a 46.5% improvement in training efficiency; and its inference time is reduced from 896.6 s/epoch in CSDI to 446.2 s/epoch, representing a 50.2% improvement in inference efficiency. These results demonstrate the superior efficiency of ZoomDiff when generating multi-scale mobile traffic.

VI. GENERATIVE MANAGEMENT OF MULTI-SCALE MOBILE TRAFFIC DATA

With the increasing demand for joint optimization across multi-level mobile networks, both operators and researchers urgently require optimization training based on massive mobile data. However, due to the privacy of traffic data and the incomplete deployment of communication infrastructure, multi-level network traffic data, especially fine-grained mobile traffic, remains difficult to obtain in many regions. Therefore, implementing full-lifecycle management of multi-scale mobile traffic based on generative AI has become an urgent need. Designed for joint generation of multi-resolution traffic, ZoomDiff demonstrates unique advantages during mobile data management, including high accessibility of input conditions, high accuracy, and high efficiency in training and inference. This section analyzes the performance of ZoomDiff from the perspectives of two key operations in mobile traffic data management: Traffic Refinement and cross-city generalization.

A. Management of Traffic Refinement

The refinement of coarse-grained traffic is an important task in mobile data management. User-level network planning often requires the estimation of grid-level network loads. However, operators can typically only obtain large-scale traffic data such as BS-level or cell-level traffic, while finer-grained traffic estimation relies on point sampling and drive testing, which suffer from limited accuracy and high cost. The pre-trained ZoomDiff model is capable of understanding the correlations among multi-scale traffic. By setting the denoising starting point of the reverse process to specific coarse-scale data, ZoomDiff can directly refine BS or cell traffic into

TABLE III: Comparison of different noise scheduling strategies on South Bank, Nanning dataset (**lower is better** for MAE/RMSE/spRMSE, **higher is better** for PSNR). Numbers in parentheses indicate variance.

Noise Sche.	N=400 (2h, BS)		N=200 (1h, Cell)				N=0 (1h, 100m grid)			
	MAE↓ e7(e4)	RMSE↓ e7(e4)	MAE↓ e7(e4)	RMSE↓ e7(e4)	spRMSE↓ e7(e4)	PSNR↑ 1(e-2)	MAE↓ e7(e4)	RMSE↓ e7(e4)	spRMSE↓ e7(e4)	PSNR↑ 1(e-2)
CN, CA, CD	30.0 (38.2)	37.4 (42.2)	17.1 (17.9)	21.3 (16.9)	35.3 (38.4)	9.67 (13.2)	2.25 (12.9)	3.32 (16.5)	2.99 (16.6)	29.4 (24.0)
CN, CA, SD	37.1 (34.1)	4.63 (36.9)	21.6 (24.6)	26.9 (22.2)	25.4 (22.1)	12.9 (10.2)	2.95 (49.1)	4.24 (57.6)	3.86 (70.0)	24.5 (49.2)
CN, SA, SD	40.1 (51.9)	50.0 (73.7)	25.1 (47.1)	31.3 (55.3)	29.6 (54.5)	14.1 (10.9)	2.91 (17.0)	4.20 (23.5)	3.79 (31.6)	26.0 (33.5)
SN, SA, CD	1.80 (24.1)	2.13 (25.6)	4.78 (90.0)	5.54 (98.7)	6.04 (97.6)	10.1 (18.8)	5.75 (126)	7.07 (127)	7.73 (156)	15.8 (65.9)
SN, SA, SD	1.80 (24.4)	2.12 (27.5)	2.14 (17.4)	2.70 (18.3)	2.60 (18.3)	19.8 (9.36)	2.17 (10.6)	3.22 (10.1)	2.91 (15.5)	29.1 (9.61)

TABLE IV: Comparison of different RGP strategies across resolution levels on the South Bank, Nanning dataset.

RGP	MAE↓ RMS e7(e4) e7(e	7 7		spRMSE, e7(e4)			RMSE↓ e7(e4)	spRMSE. e7(e4)	↓ PSNR↑ 1(e-2)		RMSE↓ e7(e4)	spRMSE↓ e7(e4)	PSNR↑ 1(e-2)
Uniform n=267 (2h, BS)		S)	n=200 (1h, Cell)			n=133 (1h, Cell)		1		00m grid)	
Ciliforni	1.84 (36.2) 2.16 (38.6) 1.82 (17.3)	2.18 (20.0)	2.09 (2.30)	17.2 (26.6)	2.01 (17.9)	2.50(19.8)	2.41 (21.9)	20.9 (29.8)	2.21 (12.7)	3.24 (16.5)	2.95 (20.1)	28.5 (20.4)
Coorse Cr	n=267 (2h, B)		-	_			n=133 (2	2h, Cell)		1	n=0 (1h, 1	00m grid)	
Coarse Gr.	1.80 (35.9) 2.12 (37.6) -	_	_	_	2.15 (16.5)	2.69 (19.3)	2.60(12.4)	19.7 (32.4)	2.19(18.8)	3.24 (18.7)	2.92 (25.3)	28.9 (28.1)
Eine Ca	n=267 (2h, B)	S)	-	_			n=133 (1h, Cell)		1	n=0 (1h, 1	00m grid)	
Fine Gr.	1.80 (24.4) 2.12 (27.5) –	-	-	-	2.14(17.4)	2.70(18.3)	2.60 (18.3)	19.8 (9.36)	2.17 (10.6)	3.22 (10.1)	2.91 (15.5)	29.1 (9.61)

TABLE V: Comparison of model efficiency.

Method	Para. Size (M)	Training Speed (s/epoch)	Inference Speed (s/epoch)
CSDI	0.748	22.9	896.6
DIT	0.99	146	1001
ZoomDiff	0.504	12.25	446.2

grid-level fine-grained traffic. Table VI presents the results of refining BS traffic into 50m grid traffic using different methods. In Table VI, *ZoomDiff (zero-shot)* directly inputs BS-level traffic into the corresponding denoising intermediate state during the reverse process, while *CSDI* and *ZoomDiff* were retrained for the traffic refinement task. The results show that *ZoomDiff (zero-shot)* achieves accuracy comparable to the retrained models, demonstrating its excellent performance in the management of traffic refinement.

TABLE VI: Comparison of BS traffic refinement.

Method	MAE↓	RMSE↓	spRMSE↓	PSNR↑
	e7(e4)	e7(e4)	e7(e4)	1(e-2)
CSDI	3.47 (12.7)	5.65 (16.5)	5.57 (20.1)	23.9 (20.4)
ZoomDiff (zero-shot)	3.54 (7.42)	5.44 (9.36)	5.67 (15.5)	23.3 (6.59)
ZoomDiff	3.24 (5.02)	5.21 (5.11)	5.17 (7.99)	24.6 (6.44)

B. Generalization Validation

Mobile data from different cities and operators is often difficult to share due to privacy concerns, which poses obstacles to multi-city mobile data management that is required for the testing of optimization strategies. Utilizing generative models to generalize the spatiotemporal distribution patterns of multi-scale traffic from known cities to unknown ones can effectively address this problem. To validate the cross-city and multi-scenario generalization capability of ZoomDiff, we conducted transfer performance tests on two cities, Nanning and Shanghai, using traffic datasets from two levels of base stations: Macro-BS (MBS) and Pico-BS (PBS). The generation

results of 1-hour granularity traffic at the PBS level are shown in Table VII. It can be observed that, compared with CSDI, ZoomDiff exhibits a relative accuracy advantage in both single-city training and cross-city transfer scenarios.

TABLE VII: Comparison of model transfer performance for PBS traffic generation. Nanning—Shanghai means training models on the Nanning dataset and testing models on the Shanghai dataset.

Method	Dataset	MAE↓ e3(e1)	RMSE↓ e3(e1)	PSNR ↑ 1(e-1)	
CSDI	Nanning Shanghai Nanning→Shanghai	1.01 (1.76) 1.88 (1.47) 2.42 (2.54)	1.28 (1.93) 2.05 (2.25) 2.87 (2.93)	19.31 (2.10) 29.11 (2.46) 26.50 (2.91)	
ZoomDiff	Nanning Shanghai Nanning→Shanghai	1.63 (2.49) 2.26 (1.08)	0.719 (0.942) 1.95 (2.61) 2.58 (1.04)	26.0 (2.89) 37.1 (1.36) 33.3 (1.49)	

VII. CONCLUSION

In this paper, we propose ZoomDiff, a diffusion-based multi-scale mobile traffic generation model. ZoomDiff employs customized multi-resolution diffusion models, DRDM. It achieves joint modeling of multi-layer network traffic with different spatial and temporal resolutions through multistage noise-adding and denoising processes. By leveraging a prior noise guidance mechanism and multi-stage denoising, ZoomDiff can simultaneously output multi-scale mobile traffic within a single denoising process by controlling the intermediate denoising states. We further explored effective noise scheduling strategies and the resolution greediness preference for DRDM. Experiments on real-world datasets demonstrate that ZoomDiff exhibits excellent performance in generating multi-scale network traffic. In addition, ZoomDiff effectively enhances the management of traffic refinement and shows strong cross-city generalization capability. This provides an effective solution for efficient generative management of multiscale mobile traffic data.

AI-GENERATED CONTENT ACKNOWLEDGEMENT

No generative AI tools were used in the conception, writing, or experimentation of this paper. All text, figures, images, and code in the paper and related materials were created entirely by the authors without the assistance of generative AI tools.

REFERENCES

- [1] X. Lyu, Y. Li, Y. He, C. Ren, W. Ni, R. P. Liu, P. Zhu, and Q. Cui, "Objective-driven differentiable optimization of traffic prediction and resource allocation for split ai inference edge networks," *IEEE Transactions on Machine Learning in Communications and Networking*, vol. 2, pp. 1178–1192, 2024.
- [2] Z. Lin, A. Jain, C. Wang, G. Fanti, and V. Sekar, "Using gans for sharing networked time series data: Challenges, initial promise, and open questions," in *Proceedings of the ACM Internet Measurement Conference*, ser. IMC '20. New York, NY, USA: Association for Computing Machinery, 2020, p. 464–483. [Online]. Available: https://doi.org/10.1145/3419394.3423643
- [3] W. Mei and R. Zhang, "Joint base station and irs deployment for enhancing network coverage: A graph-based modeling and optimization approach," *IEEE Transactions on Wireless Communications*, vol. 22, no. 11, pp. 8200–8213, 2023.
- [4] X. Wang, B. Lyu, C. Guo, J. Xu, and M. Zukerman, "A base station sleeping strategy in heterogeneous cellular networks based on user traffic prediction," *IEEE Transactions on Green Communications and Networking*, vol. 8, no. 1, pp. 134–149, 2024.
- [5] Y. Zhu and S. Wang, "Joint traffic prediction and base station sleeping for energy saving in cellular networks," in *ICC 2021 - IEEE Interna*tional Conference on Communications, 2021, pp. 1–6.
- [6] X. Lin and S. Wang, "Joint user association and base station switching on/off for green heterogeneous cellular networks," in 2017 IEEE International Conference on Communications (ICC), 2017, pp. 1–6.
- [7] Y. Qiao, Y. Niu, Z. Han, S. Mao, R. He, N. Wang, Z. Zhong, and B. Ai, "Joint optimization of resource allocation and user association in multi-frequency cellular networks assisted by ris," *IEEE Transactions* on Vehicular Technology, vol. 73, no. 1, pp. 826–842, 2024.
- [8] H. Yang, J. Zhao, K.-Y. Lam, Z. Xiong, Q. Wu, and L. Xiao, "Distributed deep reinforcement learning-based spectrum and power allocation for heterogeneous networks," *IEEE Transactions on Wireless Communica*tions, vol. 21, no. 9, pp. 6935–6948, 2022.
- [9] S. Chowdhury and A. Katangur, "Optimizing cloud computing performance through integration of a threshold-based load balancing algorithm with multiple service broker policies," *IEEE Transactions on Cloud Computing*, vol. 13, no. 2, pp. 751–768, 2025.
- [10] S. Jamshidiha, V. Pourahmadi, and A. Mohammadi, "A traffic-aware graph neural network for user association in cellular networks," *IEEE Transactions on Mobile Computing*, vol. 24, no. 8, pp. 6858–6869, 2025.
- [11] X. Chen, L. Han, M. Wang, J. Sun, Y. Gao, X. Ou, D. Zhang, and H. Li, "Intelligent network-level energy saving strategy with stgnndriven traffic prediction and path optimization in transport networks and field trial," *IEEE Access*, vol. 13, pp. 116118–116129, 2025.
- [12] K. Xu, R. Singh, M. Fiore, M. K. Marina, H. Bilen, M. Usama, H. Benn, and C. Ziemlicki, "Spectragan: spectrum based generation of city scale spatiotemporal mobile network traffic data," in *Proceedings of the 17th International Conference on Emerging Networking Experiments and Technologies*, ser. CoNEXT '21. New York, NY, USA: Association for Computing Machinery, 2021, p. 243–258. [Online]. Available: https://doi.org/10.1145/3485983.3494844
- [13] H. Chai, T. Jiang, and L. Yu, "Diffusion model-based mobile traffic generation with open data for network planning and optimization," in *Proceedings of the 30th ACM SIGKDD Conference on Knowledge Discovery and Data Mining*, ser. KDD '24. New York, NY, USA: Association for Computing Machinery, 2024, p. 4828–4838. [Online]. Available: https://doi.org/10.1145/3637528.3671544
- [14] O. Aouedi, V. A. Le, K. Piamrat, and Y. Ji, "Deep learning on network traffic prediction: Recent advances, analysis, and future directions," *ACM Comput. Surv.*, vol. 57, no. 6, Feb. 2025. [Online]. Available: https://doi.org/10.1145/3703447
- [15] Y. Yao, B. Gu, Z. Su, and M. Guizani, "Mvstgn: A multi-view spatial-temporal graph network for cellular traffic prediction," *IEEE Transactions on Mobile Computing*, vol. 22, no. 5, pp. 2837–2849, 2023.

- [16] M. Sharma, U. Pawar, A. Antony Franklin, and B. R. Tamma, "Proactive clustering of base stations in 5gc-ran using cellular traffic prediction," in 2022 IEEE 8th International Conference on Network Softwarization (NetSoft), 2022, pp. 339–347.
- [17] X. Chen, G. Han, Y. Bi, Z. Yuan, M. K. Marina, Y. Liu, and H. Zhao, "Traffic prediction-assisted federated deep reinforcement learning for service migration in digital twins-enabled mec networks," *IEEE Journal* on Selected Areas in Communications, vol. 41, no. 10, pp. 3212–3229, 2023.
- [18] D. Kim, S. Shin, J. Jeong, and J. Lee, "Joint edge server selection and data set management for federated-learning-enabled mobile traffic prediction," *IEEE Internet of Things Journal*, vol. 11, no. 3, pp. 4971– 4986, 2024.
- [19] D. Han, J. Lee, M. Kim, and Y. Lee, "Xrman: Towards real-time hand-object pose tracking in extended reality," in *Proceedings of* the 30th Annual International Conference on Mobile Computing and Networking, ser. ACM MobiCom '24. New York, NY, USA: Association for Computing Machinery, 2024, p. 1575–1577. [Online]. Available: https://doi.org/10.1145/3636534.3697422
- [20] J. Schulz, C. Dubslaff, P. Seeling, S.-C. Li, S. Speidel, and F. H. P. Fitzek, "Negative latency in the tactile internet as enabler for global metaverse immersion," *IEEE Network*, vol. 38, no. 5, pp. 167–173, 2024.
- [21] J. Wang, J. Liu, and N. Kato, "Networking and communications in autonomous driving: A survey," *IEEE Communications Surveys & Tutorials*, vol. 21, no. 2, pp. 1243–1274, 2019.
- [22] Y. Zhu, Q. Ma, C. Bisdikian, and C. Ying, "User-centric management of wireless lans," *IEEE Transactions on Network and Service Management*, vol. 8, no. 3, pp. 165–175, 2011.
- [23] M. F. Pervej, R. Jin, S.-C. Lin, and H. Dai, "Efficient content delivery in user-centric and cache-enabled vehicular edge networks with deadlineconstrained heterogeneous demands," *IEEE Transactions on Vehicular Technology*, vol. 73, no. 1, pp. 1129–1145, 2024.
- [24] B. Ayesha, B. Jeewanthi, C. Chitraranjan, A. S. Perera, and A. S. Kumarage, "User localization based on call detail record," in *Intelligent Data Engineering and Automated Learning IDEAL 2019*, H. Yin, D. Camacho, P. Tino, A. J. Tallón-Ballesteros, R. Menezes, and R. Allmendinger, Eds. Cham: Springer International Publishing, 2019, pp. 411–423.
- [25] E. Boz and J. Manner, "A hybrid approach measurements in cellular networks," Computer qos Net-107158, 2020. [Online]. works, vol. 172. p. https://www.sciencedirect.com/science/article/pii/S1389128619314240
- [26] R. B. Basat, G. Einziger, M. Mitzenmacher, and S. Vargaftik, "Faster and more accurate measurement through additive-error counters," in *IEEE INFOCOM 2020 - IEEE Conference on Computer Communications*, 2020, pp. 1251–1260.
- [27] C. D. Guerrero and M. A. Labrador, "On the applicability of available bandwidth estimation techniques and tools," *Computer Communications*, vol. 33, no. 1, pp. 11–22, 2010. [Online]. Available: https://www.sciencedirect.com/science/article/pii/S0140366409002412
- [28] K. V. Vishwanath and A. Vahdat, "Realistic and responsive network traffic generation," in Proceedings of the 2006 Conference on Applications, Technologies, Architectures, and Protocols for Computer Communications, ser. SIGCOMM '06. New York, NY, USA: Association for Computing Machinery, 2006, p. 111–122. [Online]. Available: https://doi.org/10.1145/1159913.1159928
- [29] M. C. Weigle, P. Adurthi, F. Hernández-Campos, K. Jeffay, and F. D. Smith, "Tmix: a tool for generating realistic tcp application workloads in ns-2," SIGCOMM Comput. Commun. Rev., vol. 36, no. 3, p. 65–76, jul 2006. [Online]. Available: https://doi.org/10.1145/1140086.1140094
- [30] J. Sommers and P. Barford, "Self-configuring network traffic generation," in *Proceedings of the 4th ACM SIGCOMM Conference* on *Internet Measurement*, ser. IMC '04. New York, NY, USA: Association for Computing Machinery, 2004, p. 68–81. [Online]. Available: https://doi.org/10.1145/1028788.1028798
- [31] L. Tedesco, A. Mello, D. Garibotti, N. Calazans, and F. Moraes, "Traffic generation and performance evaluation for mesh-based nocs," in Proceedings of the 18th Annual Symposium on Integrated Circuits and System Design, ser. SBCCI '05. New York, NY, USA: Association for Computing Machinery, 2005, p. 184–189. [Online]. Available: https://doi.org/10.1145/1081081.1081129
- [32] W. Heirman, J. Dambre, and J. Van Campenhout, "Synthetic traffic generation as a tool for dynamic interconnect evaluation," in Proceedings of the 2007 International Workshop on System Level

- Interconnect Prediction, ser. SLIP '07. New York, NY, USA: Association for Computing Machinery, 2007, p. 65–72. [Online]. Available: https://doi.org/10.1145/1231956.1231970
- [33] C. Pandey, V. Tiwari, A. L. Imoize, C.-T. Li, C.-C. Lee, and D. S. Roy, "5gt-gan: Enhancing data augmentation for 5g-enabled mobile edge computing in smart cities," *IEEE Access*, vol. 11, pp. 120 983–120 996, 2023.
- [34] T. Li, S. Hui, S. Zhang, H. Wang, Y. Zhang, P. Hui, D. Jin, and Y. Li, "Mobile user traffic generation via multi-scale hierarchical gan," ACM Trans. Knowl. Discov. Data, vol. 18, no. 8, Jul. 2024. [Online]. Available: https://doi.org/10.1145/3664655
- [35] S. Hui, H. Wang, Z. Wang, X. Yang, Z. Liu, D. Jin, and Y. Li, "Knowledge enhanced gan for iot traffic generation," in *Proceedings* of the ACM Web Conference 2022, ser. WWW '22. New York, NY, USA: Association for Computing Machinery, 2022, p. 3336–3346. [Online]. Available: https://doi.org/10.1145/3485447.3511976
- [36] G. Kougioumtzidis, V. K. Poulkov, P. I. Lazaridis, and Z. D. Zaharis, "Mobile network traffic prediction using temporal fusion transformer," *IEEE Transactions on Artificial Intelligence*, vol. 6, no. 10, pp. 2685–2699, 2025.
- [37] Y. Yuan, J. Ding, J. Feng, D. Jin, and Y. Li, "A universal pre-training and prompting framework for general urban spatio-temporal prediction," *IEEE Transactions on Knowledge and Data Engineering*, vol. 37, no. 5, pp. 2212–2225, 2025.
- [38] Z. Zhou, J. Ding, Y. Liu, D. Jin, and Y. Li, "Towards Generative Modeling of Urban Flow through Knowledge-enhanced Denoising Diffusion," arXiv e-prints, p. arXiv:2309.10547, Sep. 2023.
- [39] N. Sivaroopan, D. Bandara, C. Madarasingha, G. Jourjon, A. Jayasumana, and K. Thilakarathna, "NetDiffus: Network Traffic Generation by Diffusion Models through Time-Series Imaging," arXiv e-prints, p. arXiv:2310.04429, Sep. 2023.
- [40] X. Jiang, S. Liu, A. Gember-Jacobson, A. N. Bhagoji, P. Schmitt, F. Bronzino, and N. Feamster, "Netdiffusion: Network data augmentation through protocol-constrained traffic generation," *Proc. ACM Meas. Anal. Comput. Syst.*, vol. 8, no. 1, Feb. 2024. [Online]. Available: https://doi.org/10.1145/3639037
- [41] R. Li, Q. Li, Q. Zou, D. Zhao, X. Zeng, Y. Huang, Y. Jiang, F. Lyu, G. Ormazabal, A. Singh, and H. Schulzrinne, "Iotgemini: Modeling iot network behaviors for synthetic traffic generation," *IEEE Transactions on Mobile Computing*, vol. 23, no. 12, pp. 13 240–13 257, 2024.
- [42] S. Xu, M. Marwah, M. Arlitt, and N. Ramakrishnan, "STAN: Synthetic Network Traffic Generation with Generative Neural Models," arXiv eprints, p. arXiv:2009.12740, Sep. 2020.
- [43] Y. Yin, Z. Lin, M. Jin, G. Fanti, and V. Sekar, "Practical gan-based synthetic ip header trace generation using netshare," in *Proceedings of the ACM SIGCOMM 2022 Conference*, ser. SIGCOMM '22. New York, NY, USA: Association for Computing Machinery, 2022, p. 458–472. [Online]. Available: https://doi.org/10.1145/3544216.3544251
- [44] M. Zhang, H. Lin, S. Takagi, Y. Cao, C. Shahabi, and L. Xiong, "Cs-gan: Modality-aware trajectory generation via clustering-based sequence gan," in 2023 24th IEEE International Conference on Mobile Data Management (MDM), 2023, pp. 148–157.
- [45] X. Yu, J. Wang, Y. Yang, Q. Huang, and K. Qu, "Bigcity: A universal spatiotemporal model for unified trajectory and traffic state data analysis," in 2025 IEEE 41st International Conference on Data Engineering (ICDE), 2025, pp. 4455–4469.
- [46] H. Wu, X. Shen, and C. Geng, "Trajectory data publishing method with local differential privacy," in 2023 IEEE International Conference on Unmanned Systems (ICUS), 2023, pp. 1–6.
- [47] R. Li, H. He, R. Wang, S. Ruan, Y. Sui, J. Bao, and Y. Zheng, "Trajmesa: A distributed nosql storage engine for big trajectory data," in 2020 IEEE 36th International Conference on Data Engineering (ICDE), 2020, pp. 2002–2005.
- [48] Q. Yu, H. Wang, Y. Liu, D. Jin, Y. Li, L. Zhu, and J. Feng, "Mobility prediction via rule-enhanced knowledge graph," ACM Trans. Knowl. Discov. Data, vol. 18, no. 9, Oct. 2024. [Online]. Available: https://doi.org/10.1145/3677019
- [49] A. Kapp, J. Hansmeyer, and H. Mihaljević, "Generative models for synthetic urban mobility data: A systematic literature review," ACM Comput. Surv., vol. 56, no. 4, Nov. 2023. [Online]. Available: https://doi.org/10.1145/3610224
- [50] A. Züfle, D. Pfoser, C. Wenk, A. Crooks, H. Kavak, T. Anderson, J.-S. Kim, N. Holt, and A. Diantonio, "In silico human mobility data science: Leveraging massive simulated mobility data (vision paper),"

- ACM Trans. Spatial Algorithms Syst., vol. 10, no. 2, Jul. 2024. [Online]. Available: https://doi.org/10.1145/3672557
- [51] H. Amiri, S. Ruan, J.-S. Kim, H. Jin, H. Kavak, A. Crooks, D. Pfoser, C. Wenk, and A. Zufle, "Massive trajectory data based on patterns of life," in *Proceedings of the 31st ACM International Conference on Advances in Geographic Information Systems*, ser. SIGSPATIAL '23. New York, NY, USA: Association for Computing Machinery, 2023. [Online]. Available: https://doi.org/10.1145/3589132.3625592
- [52] S. Thirumuruganathan, S. Hasan, N. Koudas, and G. Das, "Approximate query processing for data exploration using deep generative models," in 2020 IEEE 36th International Conference on Data Engineering (ICDE), 2020, pp. 1309–1320.
- [53] P. Robert and Y. Escoufier, "A unifying tool for linear multivariate statistical methods: The rv-coefficient," *Journal of the Royal Statistical Society Series C: Applied Statistics*, vol. 25, no. 3, pp. 257–265, 12 2018. [Online]. Available: https://doi.org/10.2307/2347233
- [54] J. Ho, A. Jain, and P. Abbeel, "Denoising Diffusion Probabilistic Models," arXiv e-prints, p. arXiv:2006.11239, Jun. 2020.
- [55] Y. Tashiro, J. Song, Y. Song, and S. Ermon, "CSDI: Conditional Score-based Diffusion Models for Probabilistic Time Series Imputation," arXiv e-prints, p. arXiv:2107.03502, Jul. 2021.
- [56] W. Peebles and S. Xie, "Scalable diffusion models with transformers," in 2023 IEEE/CVF International Conference on Computer Vision (ICCV), 2023, pp. 4172–4182.
- [57] Z. Sheng, D. Yuan, J. Ding, and Y. Li, "Unveiling the Power of Noise Priors: Enhancing Diffusion Models for Mobile Traffic Prediction," arXiv e-prints, p. arXiv:2501.13794, Jan. 2025.
- [58] T. Chen and C. Guestrin, "Xgboost: A scalable tree boosting system," in *Proceedings of the 22nd ACM SIGKDD International Conference on Knowledge Discovery and Data Mining*, ser. KDD '16. New York, NY, USA: Association for Computing Machinery, 2016, p. 785–794. [Online]. Available: https://doi.org/10.1145/2939672.2939785
- [59] A. Vaswani, N. Shazeer, N. Parmar, J. Uszkoreit, L. Jones, A. N. Gomez, L. Kaiser, and I. Polosukhin, "Attention is all you need," in *Proceedings* of the 31st International Conference on Neural Information Processing Systems, ser. NIPS'17. Red Hook, NY, USA: Curran Associates Inc., 2017, p. 6000–6010.
- [60] J. Yoon, D. Jarrett, and M. van der Schaar, *Time-series generative adversarial networks*. Red Hook, NY, USA: Curran Associates Inc., 2019
- [61] X. Yuan and Y. Qiao, "Diffusion-TS: Interpretable Diffusion for General Time Series Generation," arXiv e-prints, p. arXiv:2403.01742, Mar. 2024.